ACS OMEGA

http://pubs.acs.org/journal/acsodf

Article

Natural Occurrence of Carbon Dots during *In Vitro* Nonenzymatic Glycosylation of Hemoglobin A0

Ashwathi Asha Madhavan, Deepak Kushwaha, Debasish Nath, Ranjita Ghosh Moulick,* and Jaydeep Bhattacharya*

Cite This: *ACS Omega* 2022, 7, 3881−3888

Read Online

ACCESS | Metrics & More | Article Recommendations

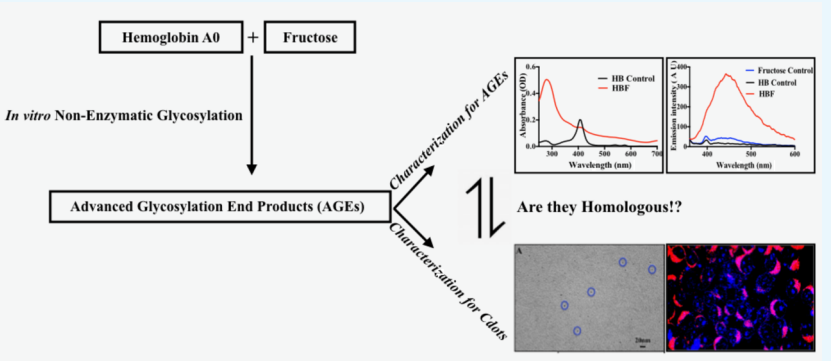

ABSTRACT: Carbon dots, the nanostructures of carbon, have excellent optical and chemical properties and find a range of applications in various fields of biology and medicine. In the current study, carbon dots are synthesized using *in vitro* nonenzymatic glycosylation at 37 °C, which is the conventional method for the synthesis of Advanced Glycosylation End products. While comparing the physicochemical properties using a series of physical and chemical analyses including light absorption, fluorescence, photoluminescence, chemical composition, functional group analysis, and *in vitro* imaging, striking similarities are found among Carbon dots and Advanced Glycosylation End products. Based on the evident resemblance between the two, we propose either the presence of a common structural backbone or the coexistence of the two individual chemical entities. Thus, the formation of carbon dots at physiological temperatures raises health concerns as nonenzymatic glycosylation is a physiological process in humans and the rate of which is elevated during diabetes. The Advanced Glycosylation End products are known to have a detrimental effect in diabetic patients, and the chemical similarity between the two questions the widely studied biocompatibility of carbon dots.

1. INTRODUCTION

Carbon dots (C dots) are nanostructures of carbon with sizes measuring below 10 nm, enriched with oxygen and/or nitrogen functionalities.[1] C dots, well known for their fluorescence and photoluminescence properties, could replace heavy metal quantum dots owing to their ease of synthesis, excellent bio- and cyto-compatibility, and cost-effectiveness.[2] The starting materials for C dot synthesis are abundantly available, and they can be conjugated with a plethora of functional molecules to enhance the chemical stability, water solubility, and quantum yield.[3] C dots were discovered accidentally during the electrophoretic purification of carbon nanotubes in 2004,[4] and these nanoscale carbon particles have gained wide popularity after its synthesis by Sun *et al.* by laser ablation of the carbon source.[5] Since then, C dots have been synthesized using different top-down and bottom-up approaches including hydrothermal methods,[6] microwave irradiation,[7] electrochemical synthesis, thermal carbonization, and acid dehydration.[8] The standout chemical and physical properties of C dots found immense applications in solar cells[9] due to the exceptional light absorption capacity, bioimaging,[10,11] biosensing employing fluorescence[12−15] and photoluminiscence properties,[15] photodynamic[16] and photothermal[17] therapy, photocatalysis,[18] temperature sensing,[19] pH sensing,[11] and electrochemical applications.[20] In addition, C dots are studied to have antimicrobial[21] properties and find theranostic applications in neurological disorders and cancer.[22]

Interestingly, some of the recent studies have found the natural presence of C dots in food sources that are rich in

Received: June 20, 2021
Accepted: August 23, 2021
Published: January 28, 2022

https://doi.org/10.1021/acsomega.1c03219
ACS Omega 2022, 7, 3881−3888

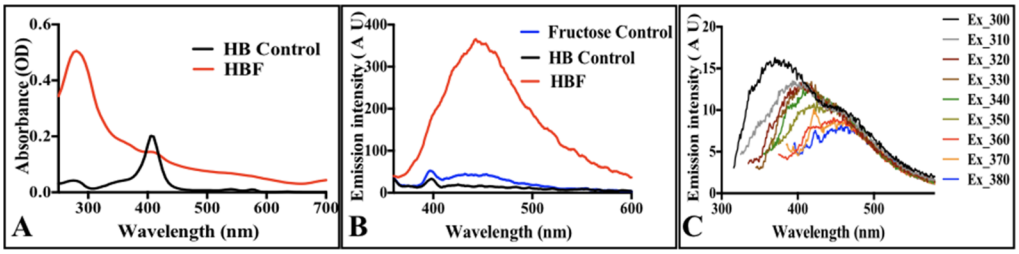

Figure 1. Spectroscopic characterization of *in vitro* nonenzymatic glycosylation: (A) UV−visible absorption spectra of HBF and HB control; (B) fluorescence emission spectra of HBF, HB control, and fructose control; and (C) photoluminiscence emission spectroscopy of HBF at increasing excitation wavelengths from 300 to 380 nm.

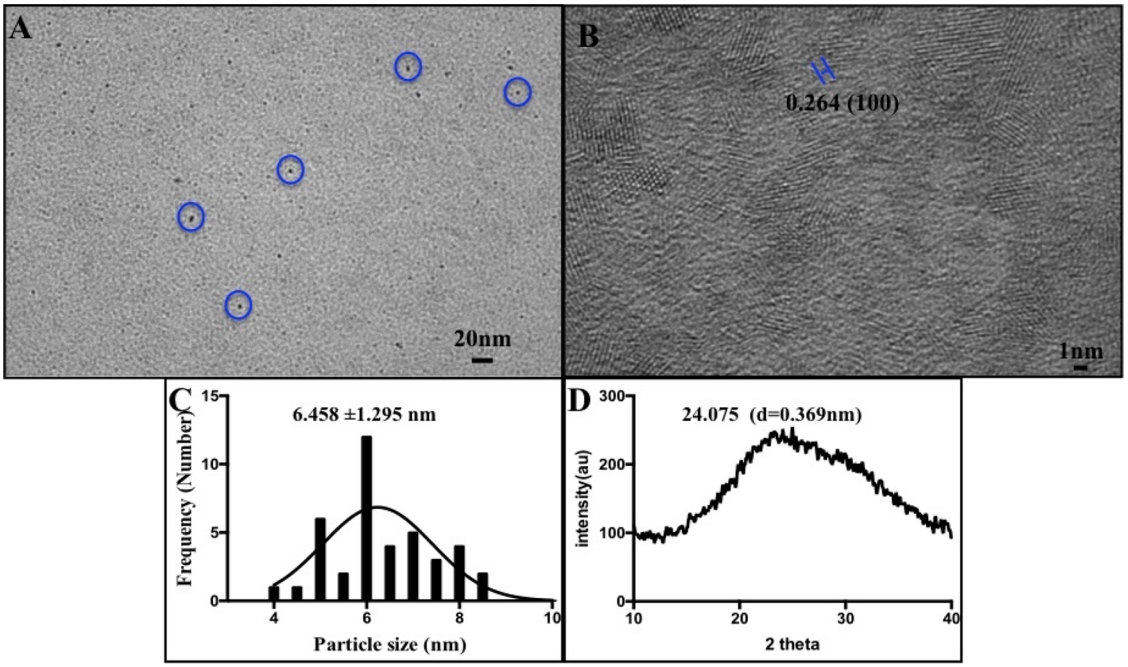

Figure 2. Morphological analysis of carbon dots in HBF: (A) TEM image, (B) HR TEM image, (C) histogram plot for particle size distribution, and (D) XRD pattern of HBF.

proteins and sugar,[23] in addition to the food products that are prepared by caramelization or browning.[24−26] The browning reaction, also known as the "Maillard reaction" or nonenzymatic glycosylation, involves the chemical reaction between reducing sugars and proteins to form highly reactive compounds rich in carbonyl functional groups,[27] which are otherwise known as Advanced Glycosylation End products (AGEs).[28,29] In 2014, Wei *et al.* for the first time reported the use of nonenzymatic glycosylation for the production of fluorescent C dots, employing glucose and amino acids as reactants in a microwave-assisted synthesis.[30] Additionally, a number of researchers reported the production of C dots using proteinaceous and sugar-rich carbon sources[6,31−33] and also from Maillard reaction products.[34]

The procedure for the *in vitro* synthesis of C dots reported in some studies[6,35,36] is strikingly similar to that of *in vitro* nonenzymatic glycosylation[27,37,38] except for the fact that the synthesis of C dots is generally performed at very high temperatures[5,7,34] to enable the rearrangement of carbon-containing functional groups. We report for the first time the spontaneous formation of C dots during *in vitro* glycosylation of Hemoglobin A0 (Hb) using fructose as a reducing sugar at 37 °C. In addition to the comparability between C dots synthesis and AGE formation through nonenzymatic glyosylation, we establish profound similarities among the properties of C dots and AGEs. Nonenzymatic glycosylation or caramelization is an inevitable flavoring process in certain food products, and concerns regarding the presence of AGEs in food derivatives are being addressed over the past years owing to their role in the pathophysiology of diabetes and associated complications.[39−41] Considering the clinical significance of AGEs[28] along with the newly found similarities with C dots, AGEs present in thermally processed foods raise serious health concerns.[42] The findings from this research can enlighten the structural and chemical aspects of both AGEs and C dots.

2. RESULTS AND DISCUSSION

2.1. *In Vitro* Nonenzymatic Glycosylation and Existence of Fluorescent C Dots. Nonenzymatic glycosylation is studied to induce significant alterations to the folded structure of proteins during the course of the reaction and formation of AGEs.[38] Figure 1A represents the UV−visible absorption spectra of HBF (Non-enzymatic glycosylated Hb) with respect to the HB control.

It shows the complete loss of the heme prosthetic group and an increase in absorbance at 280 nm (absorbance by aromatic

https://doi.org/10.1021/acsomega.1c03219
ACS Omega 2022, 7, 3881−3888

amino acids) due to postglycation unfolding of the protein structure. The unfolding of the protein is accompanied by the formation of AGEs as seen in the fluorescence emission spectra of HBF (Figure 1B). Not all but some of the identified AGEs are known to exhibit fluorescence emission in the violet−blue region of the electromagnetic spectrum and hence are used as a primary and important tool for the identification of AGEs.[46] HBF shows a significantly high fluorescence emission at 450 nm in comparison to the respective protein (HB) and sugar (fructose) controls, confirming the formation of AGEs (Figure 1B). The fluorescence emission of AGEs in the blue region of the spectrum closely resembles the emission profile of C dots synthesized from some biological sources,[32,47] and that incited us to look for the photoluminescence of *in vitro* glycated HB. Interestingly, HBF exhibited photoluminescence when excited at 350 nm and wavelengths ranging from 300 to 380 nm (Figure 1C). The ability to show fluorescence emission in a wide range of the excitation spectrum is an important and unique feature of the carbon dots[32] or quantum dots[48] in general. This enabled us to propose that since *in vitro* approaches for the synthesis of C dots involve a similar procedure to that of nonenzymatic glycosylation, there is a possibility of spontaneous formation of C dots in glycation reactions involving protein and sugar.

2.2. Evidence for the Presence of Carbon Dots in *In Vitro* Glycated HB. The spectroscopic characteristics of HBF and their comparability to those of carbon dots inspired us to investigate further the possibility of the formation of C dots in these samples. When viewed under a transmission electron microscope, HBF showed the presence of small carbonaceous particles spread throughout the sample (Figure 2A).

Also, the HR TEM image indicated a de-spacing value of 0.264 nm (Figure 2B), corresponding to the lattice points of the 100 plane of graphite,[49] as reported for carbon dots synthesized from biological sources.[50] The mean diameter of the observed particles was measured to be 6.458 nm with a standard deviation of 1.295 nm (Figure 2C). The XRD analysis of HBF showed a peak at 2θ = 24.075 that corresponds to a de-spacing value of 0.369 nm, which confirms the presence of graphitic regions in HBF.[51] The morphological features of the particles observed here in HBF are comparable to those of C dots,[51−53] and this represents the primary evidence for the presence of C dots in glycated HB samples.

Although the exact chemical structure of C dots is largely unknown and still under investigation, C dots are known to be rich in carbon- and nitrogen-based functional groups that impart them their unique spectroscopic properties.[54] To further understand the chemistry of the C dots from HBF (C dot_HBF), we evaluated the surface properties of the same. The presence of functional groups in a chemical entity largely determines the chemical reactivity of the molecule. The reducing property of HBF was measured against that of sugar and protein controls to have an idea about the functional groups present in HBF. Figure 3 shows the comparative study of the reducing properties of HBF along with HB and fructose controls.

As evident from the figure, the reducing property of HBF was significantly greater compared to its controls, indicating the presence of a large number of functional groups in HBF. The presence of carbon, nitrogen, and oxygen in HBF was confirmed using EDAX analysis (Figure 4A). The functional groups in HBF were then studied in detail using XPS. As shown in Figure 4B, the survey spectrum confirmed the

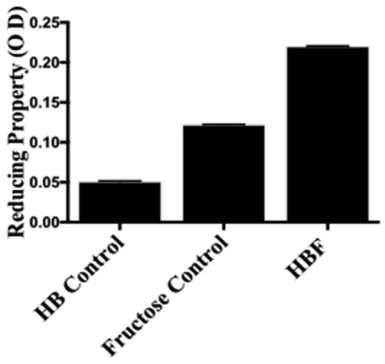

Figure 3. Reducing property analysis of HBF, HB control, and fructose control.

presence of carbon-, nitrogen-, and oxygen-based functional groups in HBF. Further evaluation of deconvoluted peaks of C 1s spectra for HBF indicated the presence of C−C/C═C (284.2 eV), C−N (285.3 eV), C−O (286.3 eV), C═O (287.2 eV), and O−C═O (289.2 eV) in HBF (Figure 4C). The O 1s spectra showed the presence of O−H (530.05 eV), *O═C−O (530.94 eV), C−O (532.07 eV), and O═C−O* (533.1 eV) (Figure 4D). The N 1s spectra showed the presence of C−N−C (398.92 eV) and N−$(C)_3$ (400.99) (Figure 4E).[34,36] Thus, XPS analysis altogether confirmed the presence of carbonyl- and carboxyl-based functional groups and primary, secondary, and tertiary amines in HBF. These functionalities present in HBF are consistent with reports on C dots.[53] This confirms the formation of C dots during the *in vitro* nonenzymatic glycosylation of HB.

2.3. Bioimaging and *In Vitro* Studies Using C Dot_HBF. One of the major advantages of carbon dots over heavy metal quantum dots in *in vivo* applications is their relatively greater cyto-compatibility compared to the latter. Carbon dots are known to be less toxic alternatives to the other heavy-metal-based quantum dots and hence are widely employed for bioimaging studies.[55−57] To study the effect of C dot_HBF in biological systems, the effect of C dot_HBF in mammalian cells (HEK293T cells) was evaluated using an MTT assay (Section 4.2.6.1). At lower concentrations, C dot_HBF increased the activity of HEK293T cells, and as the concentration increased further, it is seen to be inducing toxicity on the cells (Figure 5A).

Consistently, the FACS analysis indicated granularity changes in the cell after treatment (Figure 6) as the scattering pattern is seen to be significantly altered. Figure 6 shows the FACS analysis of untreated HEK293T cells (Figure 6A) and cells treated with increasing concentrations of C dot_HBF (Figure 6B−D). The total number of acquired events was divided into four quadrants. A shift of cell number toward Q1 shows an increase in granularity and enhanced cell death upon treatment with increasing concentrations of C dot_HBF (Figure 6B−D) when compared to the untreated control (Figure 6A). The *in vitro* studies thus confirmed that C dot_HBF induce cytotoxicity in cells at higher concentrations, which is consistent with some of the reported literature.[58,59]

To study the probability of using C dot_HBF for bioimaging, we did confocal imaging of HEK293T cells using C dot_HBF as a staining agent. A lesser concentration of C dot_HBF was used for confocal imaging compared to the FACS analysis to enable the identification of C dot_HBF as an imaging tool with minimum damage to cell morphology.

https://doi.org/10.1021/acsomega.1c03219
ACS Omega 2022, 7, 3881−3888

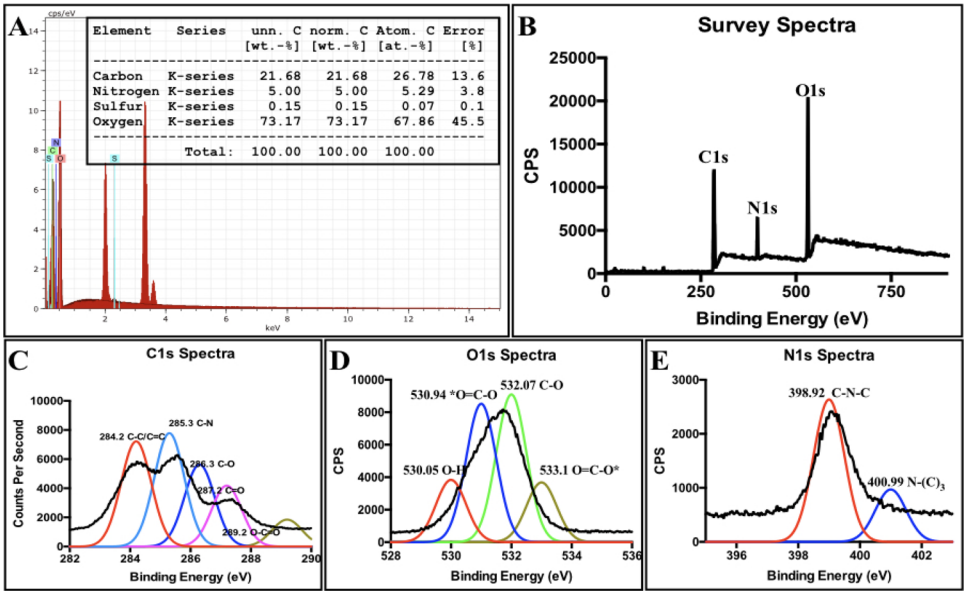

Figure 4. Elemental and functional group analysis of HBF: (A) EDAX elemental analysis, (B) XPS survey spectra, (C) C 1s spectra, (D) O 1s spectra, and (E) N 1s spectra of HBF.

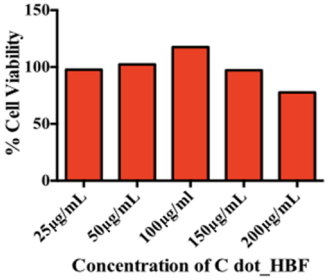

Figure 5. *In vitro* cytotoxicity studies of C dot_HBF: MTT cytotoxicity assay for C dot_HBF at increasing concentrations in HEK293T cells.

HEK293T cells were stained with C dot_HBF and either Mito Red or LysoTracker to investigate the colocalization of C dot_HBF in either of the organelles. Figures 7 and 8 represent the confocal images of HEK293T cells with Mito Red and LysoTracker along with C dot_HBF, respectively.

Upon the excitation of cells labeled with C dot_HBF, with the 4′,6-diamidino-2-phenylindole (DAPI) 405 nm filter, the cells are seen to be exhibiting blue fluorescence confirming the uptake of C dot_HBF by the cells (Figures 7B and 8B). The colocalization study revealed that the C dot_HBF were present all over the cytosol including the mitochrondia and lysosome (Figures 7D and 8D). To check whether the fluorescence of C dot_HBF has a probability of pH-dependent quenching in lysosomes and subsequent decrease in signal, we incubated the C dot_HBF in solutions of different pH and found that there is only a slight decrease in AGE fluorescence at the extreme conditions (data not shown). From the analysis of the intensities using ImageJ, it was found that C dot_HBF are colocalized in mitochondria and lysosomes with the ratios ~30.5 ± 4.5 and ~29.5 ± 5.5%, respectively. This indicates that C dot_HBF do not show subcellular localization specificity toward any of these two organelles. However, lesser localization of C dot_HBF was obtained in the nucleus.

The striking similarities among the structure, fluorescence, and photoluminescence properties and morphological features

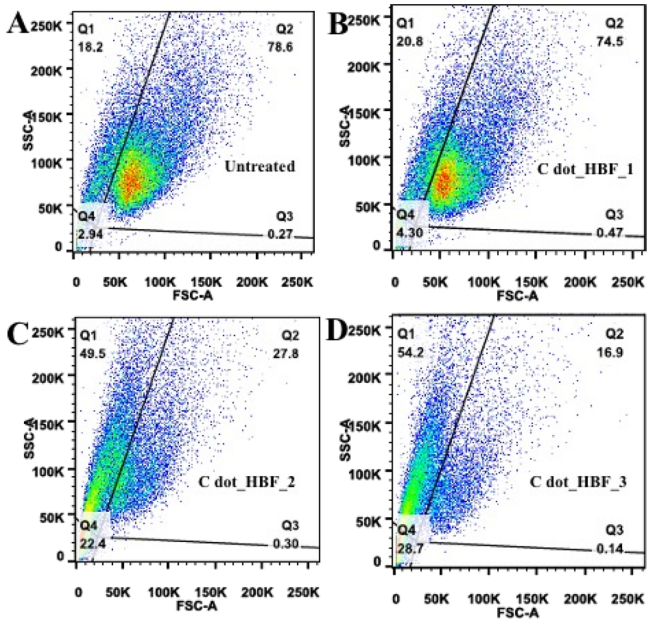

Figure 6. FACS analysis: the FSC vs SSC plots for (A) untreated HEK293T cells and (B–D) HEK293T cells treated with increasing concentrations of C dot_HBF (C dot_HBF_1, C dot_HBF_2, and C dot_HBF_3).

of C dots and AGEs are interesting phenomena(Figure 1). Although sugars and amino acids have been successfully used as a source for the production of C dots using microwave-assisted procedures, this is the first report of C dots synthesis at physiological temperatures. C dots and AGEs are either two coexisting chemical moieties produced as a result of glycation or structures with chemical similarity. They get internalized into HEK293T cells and induce morphological changes and cytotoxicity in a concentration-dependent manner *in vitro* (Figures 7 and 8). The fluorescence emission that is common to AGEs and C dots at the comparable frequencies of the electromagnetic spectrum enables the fluorescence imaging of HEK293T cells *in vitro* when administered in nontoxic

https://doi.org/10.1021/acsomega.1c03219
ACS Omega 2022, 7, 3881−3888

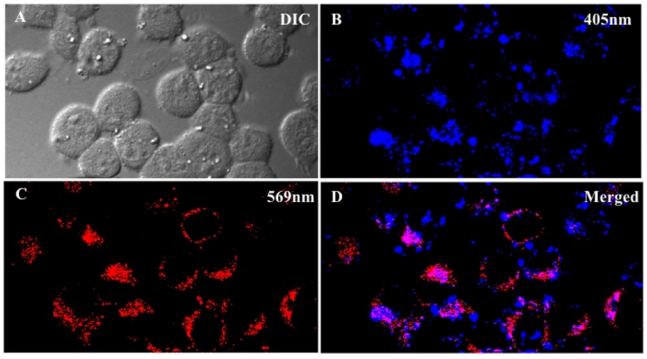

Figure 7. Confocal imaging of HEK293T cells with C dot_HBF and Mito Red: confocal images of (A) unstained, (B) C dot_HBF treated, (C) Mito Red treated, and (D) merged HEK293T cells.

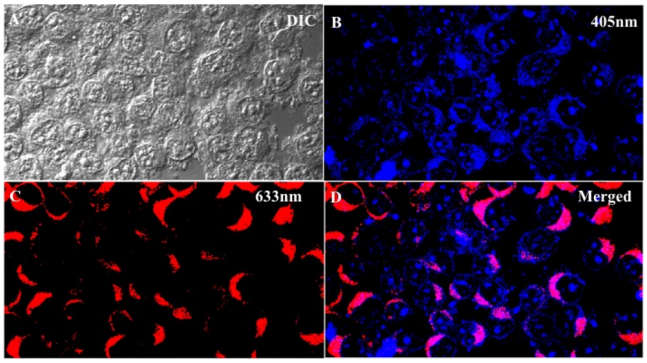

Figure 8. Confocal imaging of HEK293T cells with C dot_HBF and LysoTracker: confocal images of (A) unstained, (B) C dot_HBF treated, (C) LysoTracker treated, and (D) merged HEK293T cells.

concentrations. From the results presented here, either C dots and AGEs are two distinct entities that happen to coexist in glycated samples, or AGEs are actually the structural elements constituting the C dots. This raises a serious health concern, as the formation of AGEs and C dots is a physiological process and the production is heightened in diabetic individuals. It is well known that AGEs are a contributing factor toward the clinical complexities in diabetic individuals and that accumulation of AGEs is at times detrimental. Hence, the chemical resemblance among C dots and AGEs is of high clinical importance. C dots are found to be naturally formed in several food products that are part of routine diet.[26,60] Thus, C dots, though expected to be relatively biocompatible, may lead to hazardous complications in diabetic individuals where AGEs are generated and accumulated in the body.

3. CONCLUSIONS

The study presented here demonstrates a high chemical resemblance between C dots, the new-age quantum dots, and AGEs—the products of nonenzymatic glycosylation. They share similarities in their optical and chemical properties and can be synthesized from unique carbon sources. Though our study demonstrates striking similarities among AGEs and C dots, further studies on the structure are required to confirm this hypothesis, and it could have important implications in the study of AGEs in the pathophysiology of diabetes and the biocompatibility of C dots in general.

In conclusion, the synthetic approaches for the production of carbon dots employ relatively higher temperatures, but for the first time, we report the synthesis of carbon dots at 37 °C using the protocol for *in vitro* nonenzymatic glycosylation. Based on this evident resemblance among the physicochemical properties of AGEs and C dots, we hypothesize that they either are a mixture of two coexisting chemical entities or have a common structural backbone. Future studies on the identification and characterization of AGEs and structural analysis of carbon dots can resolve and shed light on the proposed phenomenon.

4. MATERIALS AND METHODS

4.1. Materials. Hemoglobin A0 (HB) was purchased from Sigma Aldrich India Pvt. Ltd. 3-(4,5-Dimethylthiazole-2-yl)-2,5-diphenyl tetrazolium (MTT), Mito Red, LysoTracker, potassium dihydrogen orthophosphate (KH_2PO_4), dipotassium hydrogen orthophosphate (K_2HPO_4), fructose, sodium dihydrogen orthophosphate (NaH_2PO_4), disodium hydrogen orthophosphate (Na_2HPO_4), potassium ferricyanide ($K_3[FeCN]_6$), trichloroacetic acid (TCA), hydrochloric acid (HCl), ferric chloride ($FeCl_3$), dimethyl sulfoxide (DMSO), and other chemicals used were of analytical grade and used without further purification. MilliQ ultra-pure water (>18 MΩ) was used for all the experiments.

4.2. Methods. *4.2.1. In Vitro Nonenzymatic Glycosylation.* Hemoglobin and fructose were chosen as reactants for nonenzymatic glycosylation. HB is one of the primary targets for reducing sugars under hyperglycemia associated with diabetes,[43] and fructose is reported to have a greater glycation reactivity in comparison to other reducing sugars.[44] The nonenzymatic glycosylation/glycation of HB was performed under sterile conditions in a laminar air flow hood; all the glasswares and plasticwares were autoclaved prior to use. Stock solutions of HB and fructose were prepared in a 100 mM potassium phosphate buffer (pH 7.4) and filter sterilized using 0.2 micron syringe filters. For glycation, 1 mg/mL HB was incubated with 100 mM fructose in an incubator set at 37 °C. Samples were taken after 10 days of incubation and stored at 4 °C until used. The formation of AGEs in the HBF samples was confirmed using UV−visible absorption spectroscopy and fluorescence emission spectroscopy. The controls for the glycation experiment consisted of the physical mixture of fructose and HB without incubation (HBC) and fructose alone (F).

4.2.2. Spectroscopy. AGE formation was preliminarily confirmed using UV−visible absorption spectroscopy and fluorescence emission spectroscopy. For absorption spectroscopy, HBF was diluted to a final concentration of 0.1 mg/mL and was scanned from 200 to 700 nm in a quartz cuvette of 1 cm path length at a scan rate of 240 nm/s. The spectra were recorded using a Perkin Elmer Lambda 25 UV−visible spectrometer. For fluorescence emission spectroscopy, samples were diluted to a final concentration of 0.1 mg/mL and excited at 350 nm, and the excitation and emission slits were set to 5 nm. The spectra were recorded using an Agilent Technologies Cary Eclipse fluorescence spectrophotometer in a 1 cm path length quartz cuvette. The photoluminescence of HBF was recorded by exciting at different wavelengths ranging from 300 to 400 nm. The samples were diluted to a concentration of 0.1 mg/mL, and spectra were recorded using the Agilent Technologies Cary Eclipse fluorescence spectrophotometer. All the dilutions for spectroscopy were done with the 10 mM potassium phosphate buffer of pH 7.4 at room temperature, and all the readings were taken in triplicate. All the

https://doi.org/10.1021/acsomega.1c03219
ACS Omega 2022, 7, 3881−3888

spectroscopy measurements were performed in triplicate, and consistent results were obtained.

4.2.3. Transmission Electron Microscopy (TEM). HBF was directly viewed under an electron microscope for visualizing the presence of any nanostructures of carbon postglycosylation. Copper-coated carbon grids were drop-casted with HBF without further dilution and dried overnight at room temperature prior to viewing under the microscope. The analysis was performed using a transmission electron microscope (TEM; JEOL 2100F) with an incident energy of 200 keV.

4.2.4. X-ray Diffraction Studies (XRD). The experiment was performed using X-ray diffraction (PANalytical X'pert PRO) with Cu Kα radiation (λ = 1.54 Å). Thin films of HBF were prepared on clean glass slides by repeatedly drop-casting HBF into an area of 1.5 × 1.5 cm at optimal concentrations. The prepared slides were inserted into the XRD chamber, and the patterns were observed.

4.2.5. Surface Properties and Functional Group Analysis. 4.2.5.1. Reducing Property Assay. A ferric ion reduction test was done for HBF to evaluate the presence of reducing functional groups using a method described by Gu *et al.*[45] with slight modifications. Briefly, 100 μL of HBF was allowed to react with 1 mL of potassium ferricyanide (1%) in 1 mL of the sodium phosphate buffer of pH 7.4. The reaction was carried out for 20 min in a water bath set at 50 °C. The mixture was then brought back to room temperature (RT) and mixed with 1 mL of trichloroacetic acid (10%). One milliliter from this mixture was then diluted with 1 mL of MilliQ water and mixed with 200 μL of ferric chloride (0.1%). Absorbance of the resultant mixture at 700 nm was measured using the Perkin Elmer Lambda 25 UV−visible spectrometer. The potassium phosphate buffer (10 mM, pH 7.4) was used as a negative control for the measurements. The values presented are the calculated mean for three independent readings.

4.2.5.2. Energy Dispersive X-ray Spectroscopy (EDX). Elemental analysis of HBF was performed using EDX to confirm the presence of carbon (C), nitrogen (N), and Oxygen (O). A thin film of HBF was prepared on clean glass surfaces and analyzed using scanning electron microscopy coupled with energy dispersive X-ray spectroscopy (Zeiss EVO40).

4.2.5.3. X-ray Photoelectron Spectroscopy (XPS). Functional group analysis of HBF was done with photoelectron microscopy using ESCA+ (Omicron Nanotechnology, Oxford Instrument Germany) equipped with a monochromator aluminum source (Al Kα radiation hv =1486.7 eV). The instrument was operated at 15 kV and 20 mA. The pass energy for the survey scan was 50 eV. For the analysis, thin films of the sample were prepared on clean glass slides and dried overnight before the measurement. The samples were then degassed overnight in an XPS FEL chamber to minimize the air contamination. The operating temperature of the chamber during measurement was 24 °C. The processing of data and deconvolution of C 1s, O 1s, and N 1s spectra were performed using the GraphPad Prism (6) software.

4.2.6. In Vitro Studies. 4.2.6.1. Cell Cytotoxicity by MTT Assay. HEK293T cells were treated with HBF to study any possible toxic effects induced on the cells. Cytotoxicity was determined using the 3-(4,5-dimethylthiazole-2-yl)-2,5-diphenyl tetrazolium (MTT) assay. An equal number of cells were seeded into the wells of a 96-well plate; the cells were allowed to grow for 24 h at 37 °C and then treated with HBF at different concentrations. Before treatment, HBF was subjected to gel filtration chromatography (Sephadex G25) to separate the C dots from any remaining unreacted protein fractions. After 24 h of the treatment, the cells were washed two to three times with the autoclaved 10 mM potassium phosphate buffer of pH 7.4 and then treated with the MTT solution (5 mg/mL) in a 1:10 (v/v) ratio. The treated cells were then incubated at 37 °C for 2 h, and then equal amounts of dimethyl sulfoxide (DMSO) were added into the wells to dissolve the formazan crystals. The absorbance was recorded at 570 nm, and the cell viability was calculated as follows. The values presented are the calculated mean for three independent readings.

$$\%\text{Cell viability} = \text{OD}_{570\text{nm (treated)}}/\text{OD}_{690\text{nm (control)}}*100$$

4.2.6.2. Fluorescence Activated Cell Sorting (FACS). HEK293T cells were seeded at a density of 150,000 cells/well in a 12-well tissue culture plate and allowed to grow in a humidified CO_2 incubator. After a growth period of 24 h, the spent media were discarded and fresh media with HBF (300 μg/mL) were added carefully to each well. Three different HBF samples were used that were nonenzymatically glycosylated for 10, 30, and 60 days, respectively, which showed increasing AGE fluorescence with respect to increased incubation. C dot_HBF_1, C dot_HBF_2, and C dot_HBF_3 in Figure 6 represent 300 μg/mL of day 10, 30, and 60 incubated HBF samples with increasing concentrations of AGEs. The AGE concentration in these samples expressed as the relative fluorescence at 450 nm is 227 ± 29.304, 744.19 ± 36.828, and 844.47 ± 25.146 arbitrary fluorescence units (AFU) per micromole of the protein. Cells were then allowed to grow for another 24 h. The attached cells were washed with phosphate-buffered saline (PBS) carefully and incubated at 37 °C for 5 min in 0.5 mL/well of the trypsin solution. Cells were then collected in the 1.5 mL tubes and spun for 5 min at 3000 rpm. The trypsin supernatant was discarded, and the pellet was resuspended in 300 μL of ice-cold PBS to obtain a single-cell homogeneous suspension. This suspension was then transferred to FACS tubes and immediately loaded in a FACS machine to record the data. All samples were kept on ice for the entire period of running the samples. Thirty thousand events were counted for each sample, and data were recorded based on the forward (FSC) and side scatter (SSC) properties of the cells. All the data were collected in triplicate, and the image showed in the results is a representative FSC vs SSC plot. The FlowJo software was used to process the data.

4.2.6.3. Confocal Imaging. Confocal imaging was done to study the uptake of HBF into the cells, employing their fluorescence properties, using an Olympus FluoView FV1000 laser confocal microscope. "MitoRed", a mitochondrial staining dye, and LysoTracker, a lysosome staining dye, were used as contrast agents for the confocal experiments. In short, HEK293T cells were seeded onto activated and sterilized coverslips placed in a six-well plate at a seeding density of 15,000 cells per coverslip. The cells were allowed to attach and grow for 24 h, after which the cells were treated with HBF (200 μg/mL). The treatment was done for about 24 h. Post 24 h of treatment, the cells were thoroughly washed with 10 mM phosphate buffer (pH 7.4). The cells were then stained with the contrast dyes, i.e., either mitoRed (100 nM in complete DMEM) or LysoTracker (50 nM in complete DMEM). After staining, the excess dye was washed off, and the cells on the coverslips were mounted onto a clean glass slide by placing a drop of 50% glycerol. The ends of the coverslip were sealed properly, and the slides were viewed under the microscope

https://doi.org/10.1021/acsomega.1c03219
ACS Omega 2022, 7, 3881−3888

within 1 h of preparation. The excitation wavelengths were 405, 569, and 633 nm for visualizing C dot_HBF, mitochondria, and lysosome, respectively. The imaging studies were done in triplicate, and the results were consistent across independent imaging studies. The acquired images were also analyzed by ImageJ to quantify the colocalization of C dot_HBF in mitochondria or lysosomes. The colocalization ratio was calculated as the ratio of C dot_HBF visualized in an organelle to the total C dot_HBF present in the field of the image. To improve signals and relative quantification, thresholding was done for the blue and red emissions obtained from the C dot_HBF fluorescence and the fluorescence staining was performed by lysosome and mitochondria specific dyes. All the intensities found above the threshold were normalized.

AUTHOR INFORMATION

Corresponding Authors

Ranjita Ghosh Moulick − *Amity Institute of Integrative Sciences and Health, Amity University Gurgaon, Haryana 122413, India;* orcid.org/0000-0003-1890-8458; Email: ranjita.ghoshmoulick@gmail.com

Jaydeep Bhattacharya − *School of Biotechnology, Jawaharlal Nehru University, New Delhi 110067, India;* orcid.org/0000-0001-7268-0867; Email: jaydeep@jnu.ac.in

Authors

Ashwathi Asha Madhavan − *School of Biotechnology, Jawaharlal Nehru University, New Delhi 110067, India*

Deepak Kushwaha − *School of Biotechnology, Jawaharlal Nehru University, New Delhi 110067, India; Amity Institute of Integrative Sciences and Health, Amity University Gurgaon, Haryana 122413, India*

Debasish Nath − *School of Biotechnology, Jawaharlal Nehru University, New Delhi 110067, India*

Complete contact information is available at: https://pubs.acs.org/10.1021/acsomega.1c03219

Funding

This work was supported by UGC-FRP, DST-SERB (YSS/2015/002007), DST-SERB (ECR/2015/00498), DST-PURSE, DST-BDTD, and UPE-II-JNU (0046).

Notes

The authors declare no competing financial interest.

ACKNOWLEDGMENTS

The authors thank AIRF, JNU, for the TEM, SEM-EDAX, and confocal imaging facility and Mr. Manu Vashistha, Dr. Ruchita Pal, and Dr. Neetu Singh for the guidance, respectively. The authors also thank Mr. Mohtashim Raza, MNIT, Jaipur, for helping with the XPS experiments. Ms. Ashwathi Asha Madhavan thanks DBT-JRF for the fellowship.

REFERENCES

(1) Atabaev, T. Doped Carbon Dots for Sensing and Bioimaging Applications: A Minireview. *Nanomaterials* **2018**, *8*, 342.

(2) Tuerhong, M.; Yang, X. U.; Xue-Bo, Y. I. N. Review on Carbon Dots and Their Applications. *Chinese J. Anal. Chem.* **2017**, *45*, 139−150.

(3) Song, Y.; Zhu, S.; Yang, B. Bioimaging based on fluorescent carbon dots. *RSC Adv.* **2014**, *4*, 27184−27200.

(4) Xu, X.; Ray, R.; Gu, Y.; Ploehn, H. J.; Gearheart, L.; Raker, K.; Scrivens, W. A. Electrophoretic Analysis and Purification of Fluorescent Single-Walled Carbon Nanotube Fragments. *J. Am. Chem. Soc.* **2004**, *126*, 12736−12737.

(5) Sun, Y. P.; Zhou, B.; Lin, Y.; Wang, W.; Fernando, K. A. S.; Pathak, P.; Meziani, M. J.; Harruff, B. A.; Wang, X.; Wang, H.; Luo, P. G.; Yang, H.; Kose, M. E.; Chen, B.; Veca, L. M.; Xie, S. Y. Quantum-sized carbon dots for bright and colorful photoluminescence. *J. Am. Chem. Soc.* **2006**, *128*, 7756−7757.

(6) Prasannan, A.; Imae, T. One-pot synthesis of fluorescent carbon dots from orange waste peels. *Ind. Eng. Chem. Res.* **2013**, *52*, 15673−15678.

(7) Huang, S.; Wang, L.; Huang, C.; Xie, J.; Su, W.; Sheng, J.; Xiao, Q. A carbon dots based fluorescent probe for selective and sensitive detection of hemoglobin. *Sens. Actuators, B* **2015**, *221*, 1215−1222.

(8) Esteves Da Silva, J. C. G.; Gonçalves, H. M. R. Analytical and bioanalytical applications of carbon dots. *Trends Anal. Curr. Trends Anal. Chem* **2011**, *30*, 1327−1336.

(9) Gao, N.; Huang, L.; Li, T.; Song, J.; Hu, H.; Liu, Y.; Ramakrishna, S. Application of carbon dots in dye-sensitized solar cells: A review. *J. Appl. Polym. Sci.* **2020**, *137*, 48443.

(10) Naik, G. G.; Alam, M. B.; Pandey, V.; Mohapatra, D.; Dubey, P. K.; Parmar, A. S.; Sahu, A. N. Multi-Functional Carbon Dots from an Ayurvedic Medicinal Plant for Cancer Cell Bioimaging Applications. *J. Fluoresc.* **2020**, *30*, 1−12.

(11) Guo, Z.; Jiao, Y.; Du, F.; Gao, Y.; Lu, W.; Shuang, S.; Dong, C.; Wang, Y. Facile synthesis of ratiometric fluorescent carbon dots for pH visual sensing and cellular imaging. *Talanta* **2020**, *216*, 120943.

(12) Radhakrishnan, K.; Sivanesan, S.; Panneerselvam, P. Turn-On fluorescence sensor based detection of heavy metal ion using carbon dots @ graphitic-carbon nitride nanocomposite probe. *J. Photochem. Photobiol., A* **2020**, *389*, 112204.

(13) Ghafarloo, A.; Emamali Sabzi, R.; Samadi, N.; Hamishehkar, H. Sensitive and selective spectrofluorimetric determination of clonazepam using nitrogen-doped carbon dots. *J. Photochem. Photobiol., A* **2020**, *388*, 112197.

(14) Zhang, W.; Li, N.; Chang, Q.; Chen, Z.; Hu, S. Making a cup of carbon dots for ratiometric and colorimetric fluorescent detection of Cu2+ ions. *Colloids Surf., A* **2020**, *586*, 124233.

(15) Li, H.; Yan, X.; Kong, D.; Jin, R.; Sun, C.; Du, D.; Lin, Y.; Lu, G. Recent advances in carbon dots for bioimaging applications. *Nanoscale Horiz.* **2020**, *5*, 218−234.

(16) Xu, N.; Du, J.; Yao, Q.; Ge, H.; Li, H.; Xu, F.; Gao, F.; Xian, L.; Fan, J.; Peng, X. Precise photodynamic therapy: Penetrating the nuclear envelope with photosensitive carbon dots. *Carbon* **2020**, *159*, 74−82.

(17) Shen, Y.; Zhang, X.; Liang, L.; Yue, J.; Huang, D.; Xu, W.; Shi, W.; Liang, C.; Xu, S. Mitochondria-targeting supra-carbon dots: Enhanced photothermal therapy selective to cancer cells and their hyperthermia molecular actions. *Carbon* **2020**, *156*, 558−567.

(18) Kütahya, C.; Wang, P.; Li, S.; Liu, S.; Li, J.; Chen, Z.; Strehmel, B. Carbon Dots as a Promising Green Photocatalyst for Free Radical and ATRP-Based Radical Photopolymerization with Blue LEDs. *Angew. Chem., Int. Ed.* **2020**, *59*, 3166−3171.

(19) Zhang, H.; You, J.; Wang, J.; Dong, X.; Guan, R.; Cao, D. Highly luminescent carbon dots as temperature sensors and "off-on" sensing of Hg2+ and biothiols. *Dyes Pigm.* **2020**, *173*, 107950.

(20) Jang, S.-J.; Kang, Y. C.; Roh, K. C. Preparation of activated carbon decorated with carbon dots and its electrochemical performance. *J. Ind. Eng. Chem.* **2020**, *82*, 383−389.

(21) Dong, X.; Liang, W.; Meziani, M. J.; Sun, Y.-P.; Yang, L. Carbon Dots as Potent Antimicrobial Agents. *Theranostics.* **2020**, *10*, 671−686.

(22) Ashrafizadeh, M.; Mohammadinejad, R.; Kailasa, S. K.; Ahmadi, Z.; Afshar, E. G.; Pardakhty, A. Carbon dots as versatile nanoarchitectures for the treatment of neurological disorders and their theranostic applications: A review. *Adv. Colloid Interface Sci.* **2020**, *278*, 102123.

(23) Mandani, S.; Dey, D.; Sharma, B.; Sarma, T. K. Natural occurrence of fluorescent carbon dots in honey. *Carbon* **2017**, *119*, 569−572.

(24) Sk, M. P.; Jaiswal, A.; Paul, A.; Ghosh, S. S.; Chattopadhyay, A. Presence of amorphous carbon nanoparticles in food caramels. *Sci. Rep.* **2012**, *2*, 2−5.
(25) Ve, A.; Dergisi, D.; Dinc, S.; Kara, M. Synthesis and Applications of Carbon Dots from Food and Natural Products. *Apiterapi ve Doga Dergisi.* **2018**, *1*, 33−37.
(26) Jiang, C.; Wu, H.; Song, X.; Ma, X.; Wang, J.; Tan, M. Presence of photoluminescent carbon dots in Nescafe® original instant coffee: Applications to bioimaging. *Talanta* **2014**, *127*, 68−74.
(27) Monnier, V. M.; Cerami, A. Non-enzymatic Giycosylation and Browning of Proteins in Diabetes. *Clin. Endocrinol. Metab.* **1982**, 431−452.
(28) Singh, R.; Barden, A.; Mori, T.; Beilin, L. Advanced glycation end-products: A review. *Diabetologia* **2001**, *44*, 129−146.
(29) Kennedy, L.; Lyons, T. J. Non-enzymatic glycosylation. *Br. Med. BulUm.* **1989**, *45*, 174−190.
(30) Wei, W.; Xu, C.; Wu, L.; Wang, J.; Ren, J.; Qu, X. Non-enzymatic-browning-reaction: A versatile route for production of nitrogen-doped carbon dots with tunable multicolor luminescent display. *Sci. Rep.* **2015**, *4*, 1−7.
(31) Sarswat, P. K.; Free, M. L. Light emitting diodes based on carbon dots derived from food, beverage, and combustion wastes. *Phys. Chem. Chem. Phys.* **2015**, *17*, 27642−27652.
(32) Xu, H.; Yang, X.; Li, G.; Zhao, C.; Liao, X. Green Synthesis of Fluorescent Carbon Dots for Selective Detection of Tartrazine in Food Samples. *J. Agric. Food Chem.* **2015**, *63*, 6707−6714.
(33) Yang, Z.; Li, Z.; Xu, M.; Ma, Y.; Zhang, J.; Su, Y.; Gao, F.; Wei, H.; Zhang, L. Controllable Synthesis of Fluorescent Carbon Dots and Their Detection Application as Nanoprobes. *Nano-Micro Lett.* **2013**, *5*, 247−259.
(34) Li, D.; Na, X.; Wang, H.; Xie, Y.; Cong, S.; Song, Y.; Xu, X.; Zhu, B. W.; Tan, M. Fluorescent Carbon Dots Derived from Maillard Reaction Products: Their Properties, Biodistribution, Cytotoxicity, and Antioxidant Activity. *J. Agric. Food Chem.* **2018**, *66*, 1569−1575.
(35) Qiao, L.; Sun, T.; Zheng, X.; Zheng, M.; Xie, Z. Exploring the optimal ratio of d-glucose/l-aspartic acid for targeting carbon dots toward brain tumor cells. *Mater. Sci. Eng., C* **2018**, *85*, 1−6.
(36) Wei, W.; Xu, C.; Wu, L.; Wang, J.; Ren, J.; Qu, X. Non-Enzymatic-Browning-Reaction: A Versatile Route for Production of Nitrogen-Doped Carbon Dots with Tunable Multicolor Luminescent Display. *Sci. Rep.* **2014**, *4*, 1−7.
(37) Suarez, G.; Rajaram, R.; Oronsky, A. L.; Gawinowicz, M. A. Nonenzymatic glycation of bovine serum albumin by fructose (fructation). Comparison with the Maillard reaction initiated by glucose. *J. Biol. Chem.* **1989**, *264*, 3674−3679.
(38) Asha Madhavan, A.; Juneja, S.; Sen, P.; Ghosh Moulick, R.; Bhattacharya, J. Gold Nanoparticle-Based Detection of Low Molecular Weight AGEs from In Vitro Glycated Haemoglobin A0 Samples. *Nanoscale Res. Lett.* **2018**, *13*, 1−10.
(39) Guilbaud, A.; Niquet-Leridon, C.; Boulanger, E.; Tessier, F. How Can Diet Affect the Accumulation of Advanced Glycation End-Products in the Human Body? *Foods.* **2016**, *5*, 84.
(40) Zhu, Y.; Snooks, H.; Sang, S. Complexity of Advanced Glycation End Products in Foods: Where Are We Now? *J. Agric. Food Chem.* **2018**, *66*, 1325−1329.
(41) Luevano-Contreras, C.; Chapman-Novakofski, K. Dietary advanced glycation end products and aging. *Nutrients* **2010**, *2*, 1247−1265.
(42) Uribarri, J.; Woodruff, S.; Goodman, S.; Cai, W.; Chen, X.; Pyzik, R.; Yong, A.; Striker, G. E.; Vlassara, H. Advanced Glycation End Products in Foods and a Practical Guide to Their Reduction in the Diet. *J. Am. Diet. Assoc.* **2010**, *110*, 911−916.e12.
(43) Bry, L.; Chen, P. C.; Sacks, D. B. Effects of hemoglobin variants and chemically modified derivatives on assays for glycohemoglobin. *Clin.Chem.* **2001**, *47*, 153−163.
(44) GhoshMoulick, R.; Bhattacharya, J.; Mitra, C. K.; Basak, S.; Dasgupta, A. K. Protein seeding of gold nanoparticles and mechanism of glycation sensing. *Nanomedicine* **2007**, *3*, 208−214.
(45) Gu, F.-L.; Kim, J. M.; Abbas, S.; Zhang, X.-M.; Xia, S.-Q.; Chen, Z.-X. Structure and antioxidant activity of high molecular weight Maillard reaction products from casein−glucose. *Food Chem.* **2010**, *120*, 505−511.
(46) Gu, F.; Kim, J. M.; Hayat, K.; Xia, S.; Feng, B.; Zhang, X. Characteristics and antioxidant activity of ultrafiltrated Maillard reaction products from a casein-glucose model system. *Food Chem.* **2009**, *117*, 48−54.
(47) Vasimalai, N.; Vilas-Boas, V.; Gallo, J.; de Cerqueira, M. F.; Menéndez-Miranda, M.; Costa-Fernández, J. M.; Dieguez, L.; Espina, B.; Fernandez-Arguelles, M. T. Green synthesis of fluorescent carbon dots from spices for in vitro imaging and tumour cell growth inhibition. *Beilstein J. Nanotechnol.* **2018**, *9*, 530−544.
(48) Wegner, K. D.; Hildebrandt, N. Quantum dots: bright and versatile in vitro and in vivo fluorescence imaging biosensors. *Chem. Soc. Rev.* **2015**, *44*, 4792−4834.
(49) Feng, T.; Ai, X.; Ong, H.; Zhao, Y. Dual-Responsive Carbon Dots for Tumor Extracellular Microenvironment Triggered Targeting and Enhanced Anticancer Drug Delivery. *ACS Appl. Mater. Interfaces* **2016**, *8*, 18732−18740.
(50) Wang, J.; Wang, C. F.; Chen, S. Amphiphilic egg-derived carbon dots: Rapid plasma fabrication, pyrolysis process, and multicolor printing patterns. *Angew. Chem., Int. Ed.* **2012**, *51*, 9297−9301.
(51) Li, H.; Kang, Z.; Liu, Y.; Lee, S.-T. Carbon nanodots: synthesis, properties and applications. *J. Mater. Chem.* **2012**, *22*, 24230−24253.
(52) Park, S. Y.; Lee, H. U.; Park, E. S.; Lee, S. C.; Lee, J. W.; Jeong, S. W.; Kim, C. H.; Lee, Y. C.; Huh, Y. S.; Lee, J. Photoluminescent green carbon nanodots from food-waste-derived sources: Large-scale synthesis, properties, and biomedical applications. *ACS Appl. Mater. Interfaces* **2014**, *6*, 3365−3370.
(53) Huang, S.; Yang, E.; Liu, Y.; Yao, J.; Su, W.; Xiao, Q. Low-temperature rapid synthesis of nitrogen and phosphorus dual-doped carbon dots for multicolor cellular imaging and hemoglobin probing in human blood. *Sens. Actuators, B* **2018**, *265*, 326−334.
(54) Qu, J.-H.; Wei, Q.; Sun, D.-W. Carbon dots: Principles and their applications in food quality and safety detection. *Crit. Rev. Food Sci. Nutr.* **2018**, *58*, 2466−2475.
(55) Puvvada, N.; Kumar, B. N. P.; Konar, S.; Kalita, H.; Mandal, M.; Patak, A. Synthesis of biocompatible multicolor luminescent carbon dots for bioimaging applications. *Sci. Technol. Adv. Mater.* **2012**, *13*, No. 045008.
(56) Lim, S. Y.; Shen, W.; Gao, Z. Carbon quantum dots and their applications. *Chem. Soc. Rev.* **2015**, *44*, 362−381.
(57) Huang, H.; Li, C.; Zhu, S.; Wang, H.; Chen, C.; Wang, Z.; Bai, T.; Shi, Z.; Feng, S. Histidine-derived nontoxic nitrogen-doped carbon dots for sensing and bioimaging applications. *Langmuir* **2014**, *30*, 13542−13548.
(58) Borriello, M.; Iannuzzi, C.; Sirangelo, I.; Borriello, M.; Iannuzzi, C.; Sirangelo, I. Pinocembrin Protects from AGE-Induced Cytotoxicity and Inhibits Non-Enzymatic Glycation in Human Insulin. *Cell* **2019**, *8*, 385.
(59) Kim, J.; Kim, K.-S.; Shinn, J.-W.; Oh, Y.-S.; Kim, H.-T.; Jo, I.; Shinn, S.-H. The Effect of Antioxidants on Glycated Albumin-Induced Cytotoxicity in Bovine Retinal Pericytes. *Biochem. Biophys. Res. Commun.* **2002**, *292*, 1010−1016.
(60) Sk, M. P.; Jaiswal, A.; Paul, A.; Ghosh, S. S.; Chattopadhyay, A. Presence of Amorphous Carbon Nanoparticles in Food Caramels. *Sci. Rep.* **2012**, *2*, 383.

https://doi.org/10.1021/acsomega.1c03219
ACS Omega 2022, 7, 3881−3888